Novel multicomponent functionalized biopolymers with enhanced thermal and dielectric properties

Sanjeeta Rani[1] (ORCID ID: 0000-0002-5761-2134)**, Syed Kashif Ali[2]** (0000-0002-3323-6672)**,**
Pawan Kumar[1] (0009-0001-9464-2404)**, Kunwar Sugam Anugrah[1]** (0009-0007-2981-0305)**,**
Laishram Saya[3],[4] (0009-0003-7623-2350)**, Geetu Gambhir[5]** (0000-0002-8995-9714)**, Drashya Gautam[4]** (0000-0002-3374-0465)**,**
Sunita Hooda[4] (0000-0001-8002-400X)**, Manisha Verma[1], *)** (0000-0001-9092-2081)

Abstract: A new functionalized biopolymer was obtained by modifying chitin using ethylenediaminetetraacetic acid and magnetite nanoparticles (Fe_3O_4). Thermogravimetric analysis was performed, and dielectric properties were examined. The obtained biopolymer showed better thermal stability, as evidenced by a higher onset temperature. The activation energy calculated using imaginary impedance data and Nyquist plots was found to be consistent. Moreover, the dielectric permittivity decreased rapidly with increasing frequency. At high frequencies, there was no dependence of dielectric loss on temperature and frequency. The obtained biopolymer can be used in many applications such as microwave devices, deflection yoke, high-frequency capacitors, sensors, etc.

Keywords: biopolymers, chitin, nanoparticles, magnetite, dielectric properties.

Nowe wieloskładnikowe funkcjonalizowane biopolimery o poprawionych właściwościach termicznych i dielektrycznych

Streszczenie: Otrzymano nowy funkcjonalizowany biopolimer poprzez modyfikację chityny przy użyciu kwasu etylenodiaminotetraoctowego i nanocząstek magnetytu (Fe_3O_4). Przeprowadzono analizę termograwimetryczną i zbadano właściwości dielektryczne. Otrzymany biopolimer wykazywał lepszą stabilność termiczną, o czym świadczyła wyższa temperatura początku rozkładu. Wykazano zgodność energii aktywacji obliczonej z wykorzystaniem danych dotyczących urojonej impedancji oraz na podstawie wykresów Nyquista. Przenikalność dielektryczna zmniejszała się gwałtownie wraz ze wzrostem częstotliwości. Przy wysokich częstotliwościach nie stwierdzono zależności stratności dielektrycznej od temperatury i częstotliwości. Otrzymany biopolimer można wykorzystać w wielu zastosowaniach, takich jak urządzenia mikrofalowe, jarzmo odchylające, kondensatory wysokiej częstotliwości, czujniki itp.

Słowa kluczowe: biopolimery, chityna, nanocząstki, magnetyt, właściwości dielektryczne.

Nanocomposites made of biodegradable polymers are environmentally friendly, and the method of their production is also harmless to the environment. Recently, there is a surge in interest regarding the dielectric attributes of biopolymer composites, attributed to their potential use as dielectric substances in diverse electronic devices, including microchips, transformers, and circuitry. Electrically active biopolymer composites with conductive properties are under scrutiny for a range of applications, encompassing biomedical, biological, flexible electrode creation, display technologies, biosensors, and cell structures for tissue regeneration. This motivated us to undertake the present work, wherein synthesis of a novel functionalized biopolymer material was conducted by adding ethylenediaminetetraacetic acid to chitin and then doping the organic composite with nano-

[1] Department of Physics, Acharya Narendra Dev College, University of Delhi, Govindpuri, Kalkaji, New Delhi 110019, India.
[2] Department of Chemistry, Faculty of Science, Jazan University, Jazan P.O. Box 82817, Saudi Arabia.
[3] Department of Chemistry, Sri Venkateswara College, University of Delhi, Dhaula Kuan, New Delhi 110021, India.
[4] Polymer Research Laboratory, Department of Chemistry, Acharya Narendra Dev College, University of Delhi, Govindpuri, Kalkaji, New Delhi 110019, India.
[5] Advance Chemistry Research Laboratory, Department of Chemistry, Acharya Narendra Dev College, University of Delhi, Govindpuri, Kalkaji, New Delhi 110019, India.
*) Author for correspondence: manishaverma@andc.du.ac.in

sized magnetite (Fe_3O_4) particles (MEDTA/CH). A comprehensive study of thermogravimetric measurements, impedance data and dielectric measurements were conducted for exploring the possibility of utilizing the synthesized material for diverse applications. The sample displayed improved thermal stability and delayed onset decomposition temperature. The activation energy calculated by dual approach using imaginary impedance data and Nyquist plots showed excellent agreement with each other. The dielectric permittivity showed a rapid decrease with increase in frequency. The dielectric loss showed a temperature and frequency independence at high frequencies indicating the suitability of MEDTA/CH as a promising material for numerous high-frequency applications, such as microwave devices, deflection yoke, high frequency capacitors, sensors etc.

Renewable materials called biopolymers are produced by living organisms or are their derivatives. All proteins, polysaccharides, and nucleic acids are categorized as forms of biopolymers under this classification, which is broad and encompasses a range of distinct material classes. Because of their cheap cost, non-toxicity and capacity for natural degradation, biopolymers are of major interest to the scientific as well as industrial communities for use in electronic applications [1, 2]. Biopolymers are being used in a variety of applications, including energy storage [3], thin film transistors [4], electroluminescence [5, 6], tissue engineering [7–9], biosensing wound-healing, and drug delivery [10]. Numerous attempts have been made to improve the biocompatibility and applications of biopolymers by adding metal oxide nanoparticles [11] as this significantly alters the stability and properties of the pristine materials, yet only limited number of works have been reported on chitin [12,13]. Thus, chitin (poly-(1-4)-β-N-acetyl glucosamine, CH) have been chosen [14–17] as the base material for the fabrication of an ideal dielectric material, due to its biocompatibility, biodegradability, non-toxicity, ability to be functionalized and abundance in nature. It has the molecular formula $[C_8H_{13}O_5]_n$ and structurally contains a long polymeric chain of N-acetylglucosamine. It is obtained as an amide derivative of glucose and is regarded as a complex carbohydrate. Its structure resembles that of cellulose, but each monomer has an additional acetyl amine group in lieu of one of its hydroxyl groups. The basic synthetic route comprises of establishing covalent linkages between β-(1 → 4) moieties of N-acetyl-D-glucosamine.

Several attempts have been reported in literature whereby the dielectric and magnetic properties of biopolymers/polysaccharides are tuned through the incorporation of several other agents [18–20]. Ethylene-diamine-tetraacetic acid (EDTA), amino polycarboxylic acid, is one such agent which can be used for modification of the properties of the base material. EDTA has a chemical formula $[CH_2N(CH_2CO_2H)_2]_2$ and is composed of two groups of Lewis bases: four carboxyl groups and two amino groups. It is an odorless, colorless, or white, crystalline (sand-like) powder. It can coordinate with several metal ions resulting in complex formation that chelates or locks up the metal ions, preventing them from exhibiting ionic characteristics. EDTA is used in various medical applications, laboratory analysis, food and beverage industry, water treatment etc. [21–23].

To comprehend the significance and application of the fabricated biopolymer-based material, in a wide range of biological as well as engineering functions [24], a thorough analysis of the dielectric and conductive properties is essential. Dielectric impedance spectroscopy offers a versatile measurement system for investigating the electrical properties of materials and systems across various significant parameters enabling researchers to gain a deeper understanding of complex underlying properties in a material and optimize applications. The aim of the present study is to design a multifunctional composite biopolymer-based material to meet the needs of high adsorption, nontoxicity, environmental friendliness, and cost-effectiveness with enhanced electrical properties. For this purpose, the physical and chemical characteristics of chitin were tailored [25] by doping with EDTA and then decorating them with magnetite (Fe_3O_4) particles to obtain ferrite doped nanoblend of EDTA and chitin (MEDTA/CH) respectively. The purpose of inducing magnetic properties through Fe_3O_4 particles to the material was to enhance its electrical properties and thermal stability. Such biomaterials have considerable research scope due to their wide applications in the field of electro-optic devices, ferrofluid-based rocket fuel, microwave devices, and in high-density information storage, drug delivery systems, super-capacitors etc.

To the best of our knowledge, no comprehensive studies on the MEDTA/CH biopolymer have been reported yet. Therefore, this work presents research on the modification of chitin using ethylenediaminetetraacetic acid and magnetite nanoparticles (Fe_3O_4) and thermal and dielectric properties of the obtained biopolymer. The structure and thermal properties were determined using X-ray diffraction (XRD) and thermogravimetric analysis (TGA) respectively. Moreover, real, and imaginary impedance and dielectric permittivity were measured.

EXPERIMENTAL PART

Materials

Analytical quality hydrochloric acid (35%), sodium hydroxide (97%), chitin (99%), methanol, acetic acid (35%) and ethylenediaminetetraacetic acid (EDTA) were provided by Merck. Ferrous chloride ($FeCl_3$) and ferric chloride ($FeCl_2$) were obtained from Sigma Aldrich. Double distilled water was used to produce all the standard solutions. 0.5 M HCL and 0.5 M NaOH solutions were used to adjust the pH of the solutions.
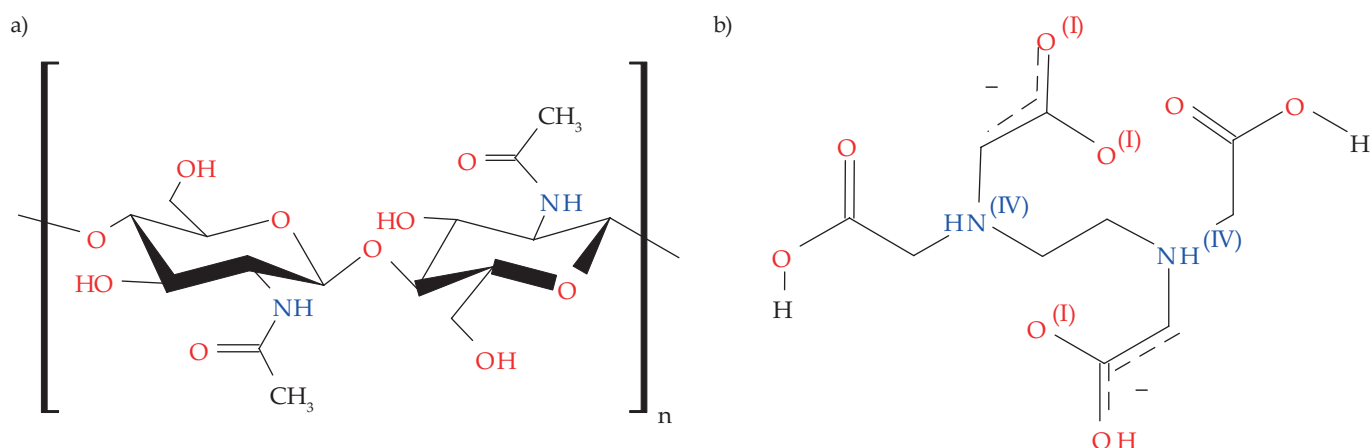
a)

b)

Fig. 1. Chemical structure: a) chitin and b) EDTA

Synthesis of EDTA/chitin (EDTA/CH)

EDTA dihydrate dissolved in methanol in a 1:1 ratio was added to a solution of chitin in an aqueous acetic acid solution (10%) and stirred at room temperature for about 24 hours. The resulting precipitate was combined with ethanol and subjected to additional stirring for a further 12 hours and then filtered. The obtained precipitate was then mixed with 0.1 M NaOH solution to reach a pH level of 11. The EDTA/CH was then filtered and washed thoroughly with water until the supernatant solution became neutral. The precipitate was then dried in a vacuum oven at 40°C for 24 hours to give a white solid. The chemical structure of CH and EDTA are shown in Fig. 1.

Synthesis of MEDTA/CH

Fe_3O_4, $FeCl_2$ and $FeCl_3$ solutions were added to the EDTA/CH precipitate described above and stirred for 1 h. The solution was filtered, and the resulting precipitate was mixed with ethanol and stirred for another 12 h. Then, 0.1 M NaOH solution was added to obtain a pH value of 11. The product (MEDTA/CH) was filtered, washed repeatedly with distilled water to obtain a neutral pH supernatant, and then dried in a vacuum oven at 40°C for 24 hours.

Methods

A Bruker D8 Discover (X Ray Source Cu, Billerica, Massachusetts, USA) was used to acquire X-ray powder diffraction spectra. The TGA HiRes 1000 thermal analyzer (Linseis, Selb, Germany) was used to evaluate thermal stability of MEDTA/CH. A nitrogen environment was maintained by a flow rate of 20 ml/min, while the powder samples were heated in an alumina pan at a constant rate of 10°C min^{-1} from 25°C to 900°C.

Using a hydraulic press with a pressure of 50 MPa, the powdered sample was pressed into disc-shaped granules with a diameter of 12 mm and a thickness of 1 mm. A thin layer of silver paste was then coated on both round

surfaces of the pellet and allowed to dry for subsequent measurements. The real and imaginary impedance and permittivity components of this compound are tested in the ranges of 1 Hz and 10 MHz, 300 K and 400 K, and bias voltages of 1 V DC using a dielectric/impedance analyzer (Novacontrol Technology, Montabaur, Germany) with an automatic data capture display.

RESULTS AND DISCUSSION

XRD analysis

The XRD patterns of the samples are presented in Fig. 2, wherein the diffraction peaks of pure CH at 2θ = 9.3° and 2θ = 19.4° and those of EDTA at 2θ = 29.2°, 37.7°, 53.3° and 57.6° are clearly visible in the XRD patterns for both EDTA/CH and MEDTA/CH, thus confirming the successful synthesis of the required nanocomposite. Additionally, the characteristic diffraction peaks of Fe_3O_4 are appearing in the MEDTA/CH diffraction pattern at angles 30.1°, 35.4°, 43.1°, 53.4°, 56.9° and 62.5°. The
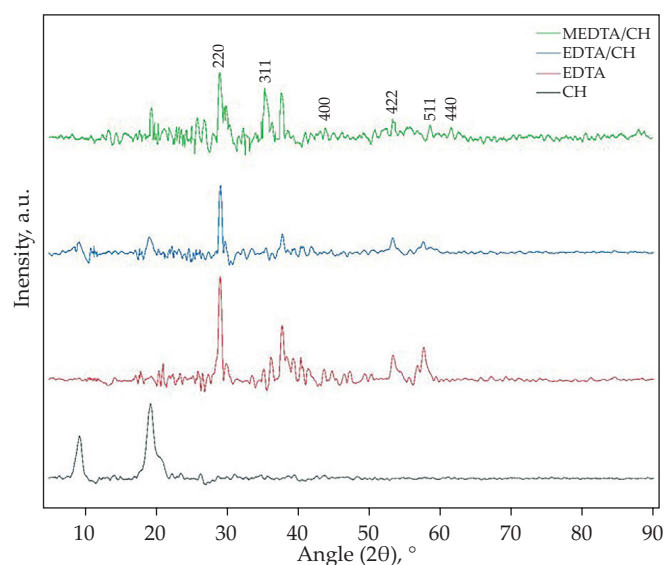

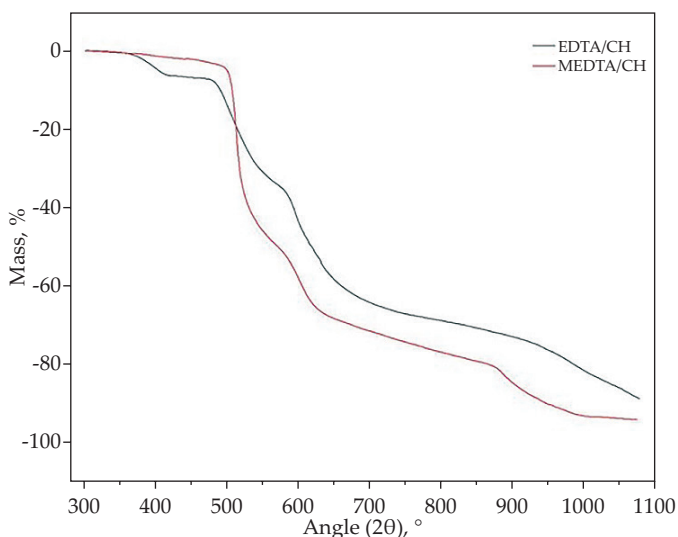Fig. 2. XRD spectra of CH, EDTA, EDTA/CH and MEDTA/CH

Sample	$T_{5\%}$, K	$T_{10\%}$, K	$T_{25\%}$, K	$T_{50\%}$, K
EDTA/CH	403.5 – 412.2	490.2 – 492.9	527.3 – 530.0	618.7 – 621.5
MEDTA/CH	499.6 – 502.1	506.6 – 507.3	514.6 – 514.7	571.4 – 576.3

peaks for Fe_3O_4 could be assigned, respectively, to [220], [311], [400], [422], [511], and [440] crystal planes (JCPDS Card No. 19-0629) [26]. It may be noted that due to weak signal/noise ratio of higher order peaks of Fe_3O_4 in this nanocomposite blended structure, these peaks could not be used in calculating the size of the particles. The size of the Fe_3O_4 particles was estimated to be ~37 nm based on the most prominent diffraction peak having Miller indices [220] shown in Fig. 2, through the Debye–Scherrer formula [27], thus confirming the successful incorporation of Fe_3O_4 nanoparticles onto EDTA/CH complex.

TGA analysis

EDTA/CH and MEDTA/CH exhibited a multistep degradation pattern as is evident from the TGA scans in Fig.3. The weight loss pattern reveals that the first and second weight degradation of 7.4%, 24.9% and 24.4% occurs at an onset temperature of 365.6 K, 477.5 K and 575.4 K respectively in the EDTA/CH sample. In contrast, pure CH is reported [28, 29] to exhibit two step degradation patterns characterized by higher weight loss. The initial weight loss is a consequence of the evaporation of the adsorbed moisture content in the sample. On the other hand, the first decomposition in the MEDTA/CH occurs at an enhanced temperature of 494.6 K wherein a loss in weight about 38.7% is seen up to 539 K. This enhancement agrees with the reported work by Hooda *et al.* [30]. A further weight loss of 16.5% is observed at an onset decomposition temperature of 563 K. Comparative TGA analysis shows that decomposition of MEDTA/CH begins at higher temperature which indicates increased thermal stability. The respective temperature ranges at which weight loss of 5%, 10%, 25% and 50% occur for both the samples are summarized in Table 1.

Impedance studies

Real impedance (Z')

The log-log plot of real impedance, Z' as a function of frequency is shown in Fig. 4, wherein it can be seen that Z' is almost flat at low frequencies and then starts decreasing rapidly with frequency. The width of this plateau region increases as the temperature increased. It is also observed that Z' decreases as the temperature increased barring 400K, where it shows an increase in comparison to its value at 390 K. Since Z' represents the resistive nature of the sample, its negative temperature coefficient confirms the semiconducting nature of the sample. Thus EDTA/CH, a functionalized biopolymer composite, becomes a semiconductor after its decoration with Fe_3O_4.

Imaginary impedance (Z")

Fig. 5 shows the log-log plot of imaginary impedance, Z" versus frequency. It is observed that Z" increases with frequency and reaches its peak value and then decreases with further rise in frequency. The peaks in Z" are obtained at all temperatures and these are observed to be shifting towards higher frequency [31] with increase in temperature.

The shift in peaks indicates involvement of a thermal process, the activation energy for which can be calculated

Fig. 3. TGA curves of EDTA/CH and MEDTA/CH
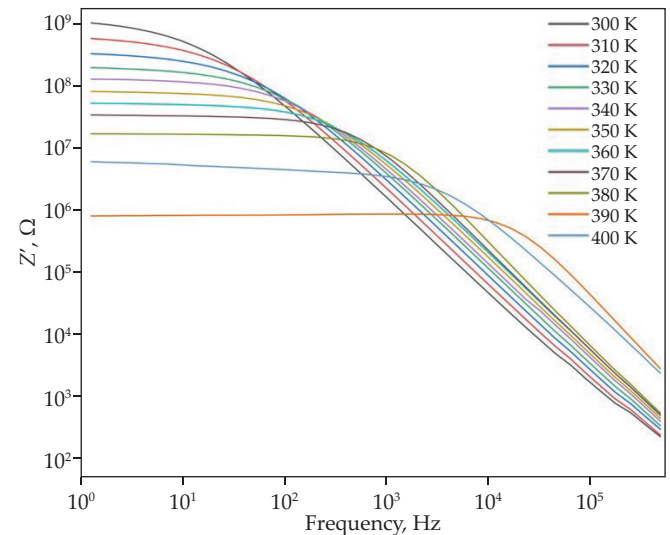
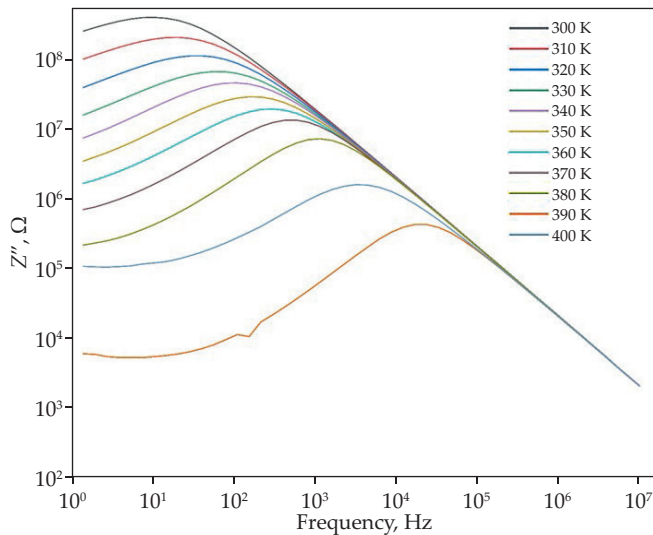Fig. 4. Plots of Z' versus frequency for MEDTA/CH

Fig. 5. Plots of Z'' versus frequency for MEDTA/CH

in the following manner. Let f_{max} be the peak position in terms of frequency at which Z'' reaches its peak Z''_{max}, then reciprocal of f_{max} will yield $\tau_{max} (= 1/f_{max})$. We plotted $\ln(\tau_{max})$ against $1/T$ and a straight line was obtained which is shown in Fig. 6. The linearity of the semi-log plot or the Arrhenius plot confirms that time constant τ_0 obeys the following relation $\tau_{max} = \tau_0 \exp(E_a/k_BT)$ where τ_0 denotes a pre-exponential factor and k_B the Boltzmann constant. Thus, the slope of the straight line can be substituted in the mentioned relation to calculate the activation energy, which was found to be 0.66 eV and is significantly high in comparison to magnetic chitin alone [32]. The increase in activation energy, when EDTA is introduced in comparison to magnetic chitin alone, suggests that EDTA plays a crucial role in modifying the material's properties due to its tendency to form strong covalent linkages [33, 34], which may contribute to the overall stability and robustness of the synthesized material. A higher activation
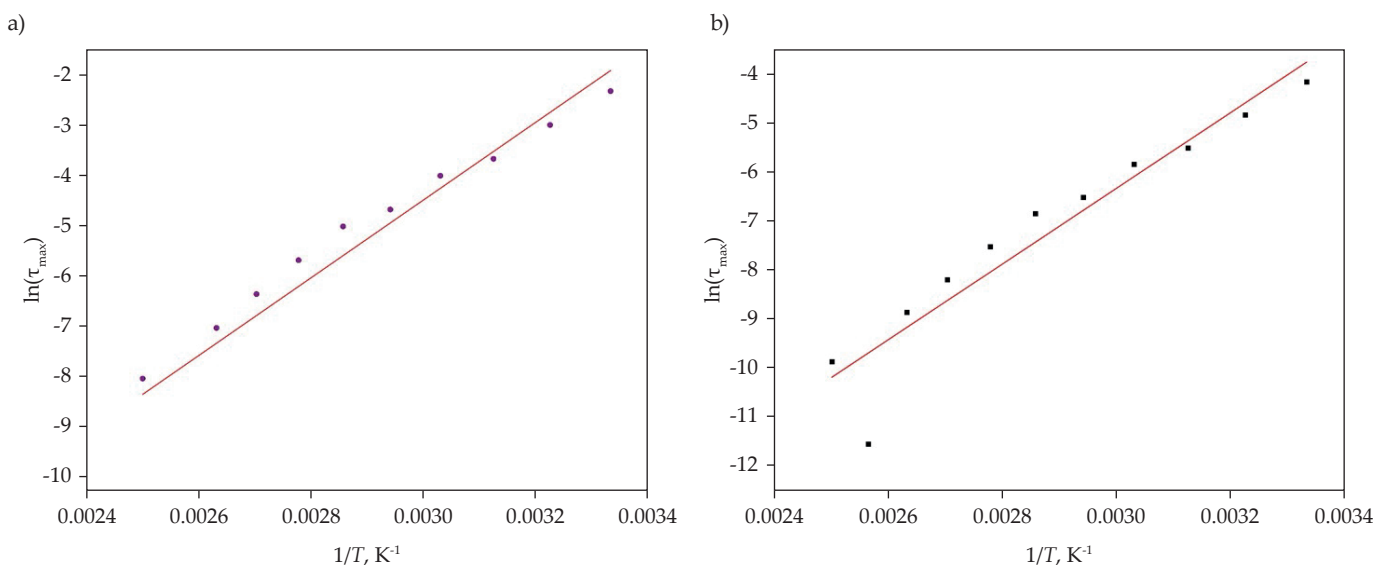
energy indicates that more energy is required to initiate a reaction or a process implying increased stability, a preferred trait in many applications [35]. Further, the role of covalent linkages in increasing activation energy underscores the significance of molecular interactions in determining material properties, thereby opening possibilities for further tuning and optimization by modifying these interactions, either by introducing new components or by altering synthesis conditions. Activation energy also plays a key role in the ionic conduction mechanism [36].

Nyquist plots

Fig. 7 depicts the Nyquist plots, which are the graphical representations of the impedance data in a complex plane. The Nyquist plots, starting from the rightmost point on the real axis and moving counterclockwise as the frequency increases, are often used to elucidate the electrical properties of materials, providing insight into the possible activation mechanism involved pertaining to the process by which charge carriers (like electrons or ions) in a material overcome certain energy barriers to conduct or move through the material. This movement is crucial for understanding the electrical and dielectric properties of the material involved. The activation energy (E_a) is a key parameter representing the energy required for charge carriers to overcome potential barriers within the material due to the inherent structure of the material and thereby contribute to the electrical conduction process at any temperature [37]. In the context of the heterogeneous composite MEDTA/CH, grain boundaries and interfaces play a significant role. Charge accumulation at these boundaries and resulting electric field can thus influence the effective activation energy significantly.

The semicircular shape of the Nyquist plot suggests that the system can be modeled in simplest way by an equivalent resistor-capacitor (*RC*) circuit, where the peak

a)

b)

Fig. 6. Arrhenius plots showing $\ln(\tau_{max})$ against $1/T$ for calculating the activation energy using: a) $-Z''$ relaxation peaks, b) R_p span from Nyquist plots for MEDTA/CH

T a b l e 2. Estimated parameters of the circuit representation of the Nyquist plots

T, K	f_{max}, Hz	τ_{max}, s	R_s, Ω	R_p, MΩ	C, F
300	10.20	$1.56 \cdot 10^{-2}$	-16.51	1053.84	$6.08 \cdot 10^{-8}$
310	19.99	$7.96 \cdot 10^{-3}$	-19.63	537.82	$2.34 \cdot 10^{-7}$
320	39.20	$4.06 \cdot 10^{-3}$	-4.89	283.20	$8.70 \cdot 10^{-7}$
330	54.88	$2.90 \cdot 10^{-3}$	-0.28	190.43	$1.81 \cdot 10^{-6}$
340	107.56	$1.48 \cdot 10^{-3}$	3.06	111.55	$6.06 \cdot 10^{-6}$
350	150.58	$1.06 \cdot 10^{-3}$	2.39	78.24	$1.21 \cdot 10^{-5}$
360	295.14	$5.39 \cdot 10^{-4}$	4.23	45.28	$4.09 \cdot 10^{-5}$
370	578.48	$2.75 \cdot 10^{-4}$	0.15	27.00	$1.35 \cdot 10^{-4}$
380	1133.82	$1.40 \cdot 10^{-4}$	3.07	15.01	$4.75 \cdot 10^{-4}$
390	16732.8	$9.51 \cdot 10^{-6}$	18.90	1.01	$1.04 \cdot 10^{-1}$
400	3111.19	$5.12 \cdot 10^{-5}$	21.50	4.30	$4.54 \cdot 10^{-3}$

corresponds to the maximum absolute value of the imaginary impedance, and a common relation in dielectric spectroscopy $\omega\tau_{max} = 1$ is fulfilled, which can be used to determine τ_{max}. The parallel resistance, R_p, in the equivalent RC circuit can be deduced from the diameter of the semi-circle in the Nyquist plot. Now using the relation $\tau_{max} = 1/R_pC$, the capacitance (C) in the equivalent RC circuit can be calculated [38,39]. From this τ_{max}, as determined from the Nyquist plot, we estimated the activation energy (E_a) again using the formula $\tau_{max} = \tau_0 \exp(E_a/k_BT)$ and it was found to be 0.67 eV. The close match between the two calculations of E_a validates the methodology and the estimation of R_p from the radii of the semicircles in the Nyquist plots in view of the non-availability of the low frequency intercept, which may be attributed to grain boundaries/interfaces. In a heterogeneous composite like MEDTA/CH, the charge accumulation at the grain boundaries or interfaces may cause non ideal behavior. The accumulated charge at the grain boundary may cause an electric field, which may lead to weakening polarization effect in the grain interior [40]. In such a scenario, grain boundaries and interfaces can mask the true intrinsic properties of the bulk material. Table 2 lists various parameters deduced from the Nyquist plots as shown in Fig. 7.

It may be seen from the table that the real part of the impedance, Z' which is represented by the series resistance (R_s), is negative initially, suggesting inductive effects at low temperatures and becomes positive as the temperature increases. It may further be noted that as the temperature increases the capacitance increases. Thus, the system seems to transit from a predominantly inductive to a capacitive behavior, as the temperature rises. It may also be seen that the estimated capacitance values range widely from 10^{-8} to 10^{-3} F, which may be related to various phenomena involving surface layers ($10^{-9} \leq C \leq 10^{-7}$) from 300–320 K, surface-electrode interface ($10^{-7} \leq C \leq 10^{-5}$) from 330–360 K and electrochemical reactions ($C \geq 10^{-4}$) from 370–400K [32].

Further, it can be seen from Fig.7 that the diameter of the semicircular arcs i.e., R_p decreases with increase in temperature. The decline of resistances with rising temperature is suggestive of semiconducting behaviors characterized by a negative temperature coefficient of resistance [41,42]. The observed electrical process in the material appears to involve a singular relaxation process, as evidenced by the presence of a single semicircle in the impedance pattern at each temperature. With increase in temperature, the center of the semicircular arc is also found shifting towards the origin indicating decrease in R_s with increase in temperature [43].

Dielectric studies

Real and imaginary permittivity

The real part of the dielectric constant (ε') with respect to frequency on a logarithmic x-axis at different temperatures ranging from 300–400 K is shown in Fig. 8. The ε'
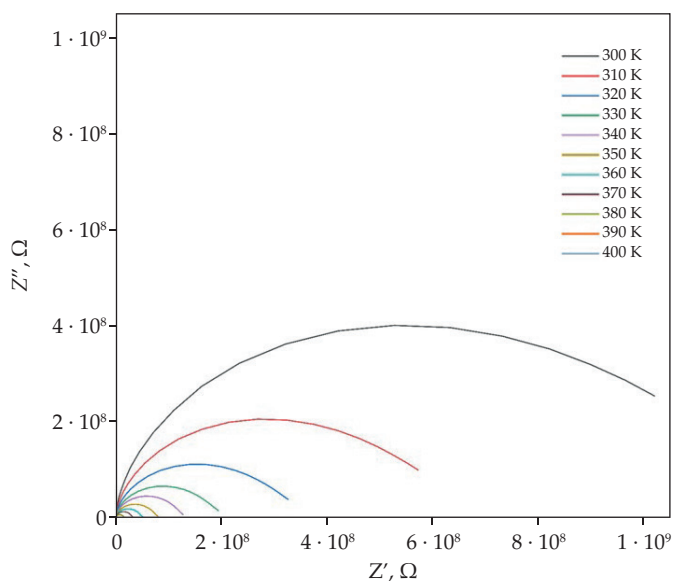
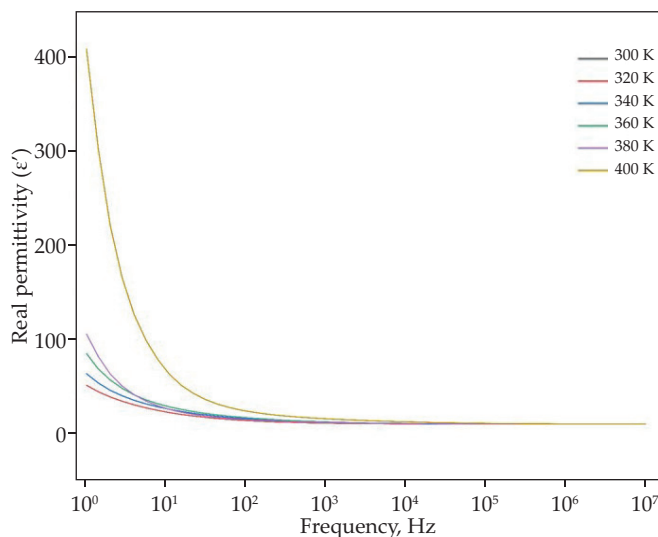**Fig. 7. Nyquist plots showing real and imaginary components of impedance at different temperatures for MEDTA/CH**

Fig. 8. Plots of real permittivity (ε') versus frequency for MEDTA/CH

Fig. 9. Plots of imaginary permittivity (ε'') versus frequency for MEDTA/CH

starts at a higher value at low frequencies and decreases as the frequency increases for all temperatures. At low frequencies, dipoles in the material have sufficient time to align themselves with the alternating electric field, leading to higher polarization and consequently a higher value of ε' is obtained. Further it may be observed from the figure that as the temperature increases, the curves shift upwards, especially noticeable at lower frequencies. This suggests that the material's polarization capabilities improve with rising temperature, possibly due to increased mobility or number of dipoles that can respond to the electric field [44]. The noticeable spike in ε' within the range of 380–400 K might be attributed to the onset of thermally induced electrochemical reactions in the material. This notion aligns with the capacitance values, $C \geq 10^{-4}$ F, derived from earlier discussed Nyquist plots and listed in Table 2. The increased ε' at elevated temperatures positions MEDTA/CH as a potential biopolymer candidate for energy storage applications.

The variation of imaginary permittivity (ε'') with frequency shown in Fig. 9 is qualitatively like that of ε', though the magnitude of ε'' is significantly higher than that of ε' with frequency as shown in Fig. 8. The values of ε' and ε'' at certain representative frequencies in the temperature range 300–400 K are listed in Table 3. It can be seen from Table 3 that although qualitative response of both the components ε' and ε'' is almost similar, quantitatively, there is a slight variation between the two. At elevated frequencies (>10 kHz), though there's negligible change in ε' with varying temperatures, Table 3 indicates a modest but consistent rise in ε'' across all frequencies, particularly up to 1 MHz. This suggests that the indifference of ε'' to temperature begins at frequencies approximately 1MHz and beyond, whereas for the real permittivity, this onset occurs at around 10 kHz.

Dielectric loss

Dielectric loss (tan δ) is defined to be the ratio of the imaginary permittivity (ε'') to real permittivity (ε'). A high value of tan δ indicates that the material is not very efficient at storing electrical energy and will dissipate more of it as heat. In contrast, a low value indicates that the material is more efficient and will have less

T a b l e 3. Values of ε' and ε'' at different temperatures and frequencies

Frequency Hz	Real permittivity (ε')						Imaginary permittivity (ε'')					
	300 K	320 K	340 K	360 K	380 K	400 K	300 K	320 K	340 K	360 K	380K	400K
10^7	9.51	9.50	9.55	9.55	9.53	9.51	-0.07	-0.023	0.014	0.020	0.014	0.10
10^6	9.55	9.40	9.47	9.48	9.46	9.55	0.031	0.041	0.054	0.064	0.065	0.29
10^5	10.1	9.47	9.57	9.61	9.58	10.1	0.070	0.11	0.17	0.24	0.27	1.31
10^4	11.80	9.69	9.89	10.1	9.98	11.8	0.20	0.40	0.65	1.03	1.48	6.34
10^3	15.2	10.5	11.1	11.8	11.1	15.2	0.81	1.78	3.12	5.50	11.6	44.6
10^2	24.3	13.5	15.5	16.6	14.5	24.3	3.76	9.46	18.9	40.1	111.0	397
10^1	78.1	23.9	27.8	31.0	28.8	78.0	22.3	65.9	156	373	1130	3510

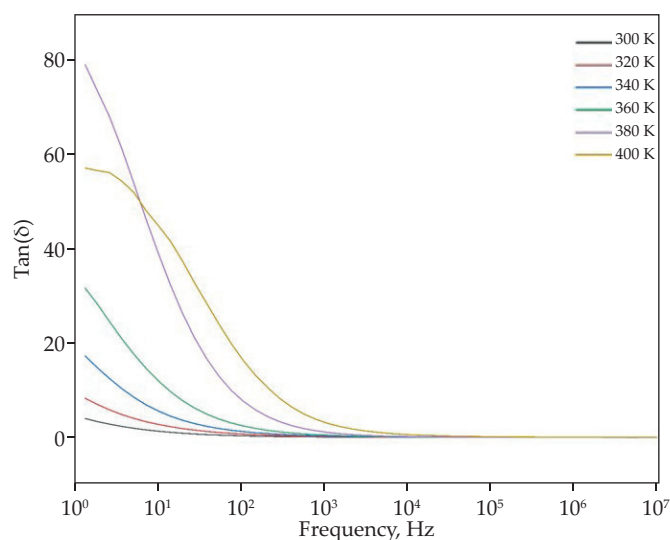**Fig.10. Dielectric loss tan (δ) versus frequency for MEDTA/CH**

energy dissipation. In practical applications, especially at high frequencies, it is essential to choose materials with low dielectric losses to prevent excessive heating and reduce energy waste. The behaviour of the dielectric loss in our biopolymers (MEDTA/CH) with respect to frequency and temperature is shown in Fig.10, which can be analyzed as follows.

Frequency dependence

The dielectric loss decreasing with an increase in frequency up to about 10 kHz, suggests that the material's tendency to dissipate energy as heat diminishes as the frequency goes up. This may be attributed to the inability of the polarization mechanisms to respond quickly enough to the changing electric field at higher frequencies [45]. This may be correlated with the decrease in real permittivity ε' indicating increase in energy storage capacity of the material as the frequency goes up till about10 kHz. Dielectric loss, tan δ, becomes almost independent of frequency beyond about 10 kHz. This may again be due to complete inability of the dipoles to orient with the alternating electric field at too fast a rate.

Temperature dependence

The increase in dielectric loss with temperature at low to medium frequencies (up to about 10 KHz) suggests that there are temperature-dependent mechanisms contributing to the energy dissipation. This could be due to increased molecular motion or other thermally activated processes that enhance the dielectric loss at these frequencies. Additionally, upon examining Fig. 10, there appears to be a discontinuity in behavior between 380–400 K for this frequency range. Such behavior might be attributed to the initiation of thermally activated electrochemical reactions within the material. This conjecture aligns with the capacitance values, $C \geq 10^{-4}$ F, noted

in Table 2 for this temperature spectrum, suggesting the presence of electrochemical reactions [32].

However, beyond 10 KHz, the convergence of the graphs at different temperatures indicates a transition to a regime where these temperature-dependent mechanisms are no longer dominant, making the dielectric loss largely temperature-independent. This temperature and frequency independence of dielectric loss at high frequencies >10 KHz makes MEDTA/CH a promising material for high-frequency electronic device applications [46, 47]. At these frequencies, the performance of the device would remain consistent across a range of temperatures, which is a desirable trait in many electronic applications.

CONCLUSIONS

EDTA/CH and MEDTA/CH functionalized biopolymers were effectively synthesized, with their structures validated by X-ray diffractograms. The thermal gravimetric (TG) curves highlighted the superior stability of MEDTA/CH over EDTA/CH, emphasizing Fe_3O_4's role in postponing the initial decomposition temperature. A detailed analysis was undertaken on the obtained impedance spectroscopic data. The real impedance, Z', exhibited a decline with both rising frequency and temperature, pointing towards the semiconducting nature of the created biopolymers. The imaginary impedance, Z", initially escalated with frequency, peaked, and subsequently reduced with a continued frequency increase. This peak exhibited a consistent shift to higher frequencies as the temperature increased, suggesting a temperature-dependent mechanism. The deduced activation energy, E_a, from the imaginary impedance stands at 0.66 eV. The semicircular trajectory of the Nyquist plots, paired with a decreasing radius as temperature elevates, reconfirmed the biopolymers' semiconducting behavior. ε' and ε" display similar responses against frequency, albeit ε" boasts a significantly larger magnitude. Additionally, a decline in dielectric loss with ascending frequency is observed, registering values <1 at ~10 kHz. Given the consistent dielectric loss at high frequencies exceeding 10 kHz irrespective of temperature and frequency, MEDTA/CH emerges as a potential candidate for high-frequency electronic devices.

REFERENCES

[1] Lv J., Lv X., Ma M. *et al.*: *Carbohydrate Polymers* **2023**, *299*, 120142.
https://doi.org/10.1016/j.carbpol.2022.120142
[2] Vinodh R., Sasikumar Y., Kim H.J. *et al.*: *Journal of Industrial and Engineering Chemistry* **2021**, *104*, 155.
https://doi.org/10.1016/j.jiec.2021.08.019

[3] Wang C., Yokota T., Someya T.: *Chemical Reviews* **2021**, *121(4)*, 2109.
https://doi.org/10.1021/acs.chemrev.0c00897

[4] Mittal P., Yadav S., Negi S.: *Materials Science in Semiconductor Processing* **2021**, *133*, 105975.
https://doi.org/10.1016/j.mssp.2021.105975

[5] Cui C., Fu Q., Meng L. *et al.*: *ACS Applied Biomaterials* **2021**, *4(1)*, 85.
https://doi.org/10.1021/acsabm.0c00807

[6] Ha J.M., Hur S.H., Pathak A. *et al.*: *NPG Asia Materials* **2021**, *13(1)*, 53.
https://doi.org/10.1038/s41427-021-00318-8

[7] Raghavan A., Ghosh S.: *Chemistry Select* **2021**, *6(47)*, 13647.
https://doi.org/10.1002/slct.202103291

[8] Asghari F., Samiei M., Adibkia K. *et al.*: *Artificial Cells, Nanomedicine, and Biotechnology* **2017**, *45(2)*, 185.
https://doi.org/10.3109/21691401.2016.1146731

[9] Bhaskar B., Nagarjuna V.: "Biomaterials, Tissue Engineering, and Regenerative Medicine: A Brief Outline" in "Biomaterials in Tissue Engineering and Regenerative Medicine", Springer Singapore 2021. p. 3.
https://doi.org/10.1007/978-981-16-0002-9_1

[10] Hasnain M.S., Ahmed S.A., Alkahtani S. *et al.*: "Biopolymers for Drug Delivery" in "Advanced Biopolymeric Systems for Drug Delivery", Springer Cham, Switzerland 2020, p. 1.
https://doi.org/10.1007/978-3-030-46923-8_1

[11] Kaushik A., Solanki P.R., Ansari A.A. *et al.*: *Sensors and Actuators B*: *Chemical* **2009**, *138(2)*, 572.
https://doi.org/10.1016/j.snb.2009.02.005

[12] Ramesan M.T., Privya P.P., Jayakrishnan P. *et al.*: *Polymer Composites* **2018**, *39(S1)*, E540.
https://doi.org/10.1002/pc.24688

[13] Ramesan M.T., Subburaj M., Mathew G., Bahuleyan B.K.: *Journal of Thermoplastic Composite Materials* **2023**, *36(3)*, 984.
https://doi.org/10.1177/08927057211046282

[14] Kumar M.N.R.: *Reactive and Functional Polymers* **2000**, *46(1)*, 1.
https://doi.org/10.1016/S1381-5148(00)00038-9

[15] Hu X., Ricci S., Naranjo S. *et al.*: *Molecules* **2021**, *26(15)*, 4499.
https://doi.org/10.3390/molecules26154499

[16] Ikram R., Jan B.M., Qadir M.A. *et al.*: *Polymers* **2021**, *13(19)*, 3266.
https://doi.org/10.3390/polym13193266

[17] Safarzadeh M., Sadeghi S., Azizi M. *et al.*: *International Journal of Biological Macromolecules* **2021**, *183*, 235.
https://doi.org/10.1016/j.ijbiomac.2021.04.157

[18] Bhatt A.S., Bhat D.K., Santosh M.S.: *Physica B: Condensed Matter* **2010**, *405(8)*, 2078.
https://doi.org/10.1016/j.physb.2010.01.106

[19] Simoes R., Silva J., Lanceros-Mendez S., Vaia R.: *Journal of Materials Science* **2010**, *45*, 268.
https://doi.org/10.1007/s10853-009-3937-2

[20] Elsawy M.A., Saad G.R., Sayed A.M.: *Polymer Engineering and Science* **2016**, *56(9)*, 987.
https://doi.org/10.1002/pen.24328

[21] Shahid M., Austruy A., Echevarria G. *et al.*: *Soil and Sediment Contamination: An International Journal* **2014**, *23(4)*, 389.
https://doi.org/10.1080/15320383.2014.831029

[22] Sun B., Zhao F.J., Lombi E. *et al.*: *Environmental pollution* **2001**, *113(2)*, 111.
https://doi.org/10.1016/S0269-7491(00)00176-7

[23] Oviedo C., Rodríguez J.: *Quimica Nova* **2003**, *26*, 901.
https://doi.org/10.1590/S0100-40422003000600020

[24] Kanagathara N., Sankar S., Saravanan L. *et al.*: *Advances in Condensed Matter Physics* **2022**, Article ID: 6002025.
https://doi.org/10.1155/2022/6002025

[25] Rogovina S.Z., Alexanyan C.V., Prut E.V.: *Journal of Applied Polymer Science* **2011**, *121(3)*, 1850.
https://doi.org/10.1002/app.33477

[26] Liu Z., Wang J., Xie D. *et al.*: *Small* **2008**, *4(4)*, 462.
https://doi.org/10.1002/smll.200701018

[27] Holzwarth U, Gibson N.: *Nature Nanotechnology* **2011**, *6*, 534.
https://doi.org/10.1038/nnano.2011.145

[28] Jayakumar R., Selvamurugan N., Nair S. V. *et al.*: *International Journal of Biological Macromolecules* **2008**, *43(3)*, 221.
https://doi.org/10.1016/j.ijbiomac.2008.07.004

[29] Shankar S., Reddy J. P., Rhin J.W. *et al.*: *Carbohydrate Polymers* **2015,** *117*, 468,
https://doi.org/10.1016/j.carbpol.2014.10.010

[30] Hooda S., Rani S., Raj V.B. *et al.*: *Rasayan Journal of Chemistry* **2023**,*16(3)*, 1495.
http://doi.org/10.31788/RJC.2023.1638445

[31] Triyono D., Supriyadi Y., Laysandra, H.: *Journal of Advanced Dielectrics* **2019**, *9(4)*, 950029.
https://doi.org/10.1142/S2010135X19500292

[32] Rani S., Hooda S., Dheer N. *et al.*: *Applied Chemical Engineering* **2023**, *6(1)*, 59.
https://doi.org/10.24294/ace.v6i1.1965

[33] Dong J., Li B., Xiao J. *et al.*: *Carbon* **2022**, *199*, 151.
https://doi.org/10.1016/j.carbon.2022.07.035

[34] Guan X., Yuan X., Zhao Y. *et al.*: *Science of The Total Environment* **2022**, *838*, 155693.
https://doi.org/10.1016/j.scitotenv.2022.155693

[35] Ambrosio R., Carrillo A., Mota M.L. *et al.*: *Polymers* **2018**, *10(12)*, 1370.
https://doi.org/10.3390/polym10121370

[36] Sengupta P., Sadhukhan P., Ray A. *et al.*: *Journal of Alloys and Compounds* **2022**, *892*, 162216.
https://doi.org/10.1016/j.jallcom.2021.162216

[37] Bendahhou A., Chourti K., El Bouayadi R. *et al.*: *RSC Advances* **2020**, *10(47)*, 28007.
https://doi.org/10.1039/D0RA05163B

[38] Batoo K.M., Kumar S., Lee C.G. *et al.*: *Current Applied Physics* **2009**, *9(5)*, 1072.
https://doi.org/10.1016/j.cap.2008.12.002

[39] Ponpandian N., Balaya P., Narayanasamy A.: *Journal of Physics: Condensed Matter* **2002**, *14(12)*, 3221.
https://doi.org/10.1088/0953-8984/14/12/311

[40] Guo W.X., Tan P.F., Ouyang X.P. *et al.*: *AIP Advances* **2018**, *8(10)*, 101336.
https://doi.org/10.1063/1.5043049

[41] Ghosh P., Bhowmik R.N., Das M.R., Mitra P.: *Physica E: Low-dimensional Systems and Nanostructure* **2017**, *88*, 218.
https://doi.org/10.1016/j.physe.2017.01.019

[42] Pearson G.L.: *Electrical Engineering* **1947**, *66*(7), 638.

[43] Chanu L.P., Phanjoubam S.: *Journal of Materials Science: Materials in Electronics* **2022**, *33(9)*, 6107.
https://doi.org/10.1007/s10854-022-07788-8

[44] Thakur A., Mathur P., Singh M.: *Journal of Physics and Chemistry of Solids* **2007**, *68(3)*, 378.
https://doi.org/10.1016/j.jpcs.2006.11.028

[45] Yang K., Huang X., Huang Y. *et al.*: *Chemistry of Materials* **2013**, *25(11)*, 2327.
https://doi.org/10.1021/cm4010486

[46] Singh C., Bai Y., Mishra S.R. *et al.*: *Applied Physics A* **2022**, *128(9)*, 820.
https://doi.org/10.1007/s00339-022-05974-3

[47] Chahar D., Taneja S., Thakur P., Thakur A.: *Journal of Alloys and Compounds* **2020**, *843*, 155681.
https://doi.org/10.1016/j.jallcom.2020.155681

Uniwersytet Rzeszowski
i
Politechnika Rzeszowska
zapraszają do udziału w

III Konferencji Naukowej Technologie w Medycynie
Medycyna 4.0
19–20 października 2023 r., Rzeszów

We współczesnej nauce i w codziennym życiu obserwujemy niezwykle dynamiczny rozwój nowoczesnych technologii zmieniających oblicze medycyny. Powstanie Klastra „Technologie w Medycynie" w oparciu o Rzeszowskie Uczelnie i środowisko biznesu jest dowodem zrozumienia tych zjawisk.

Celem konferencji jest przybliżenie studentom inżynierii medycznej, doktorantom, młodym biznesmenom oraz osobom, które planują stworzenie własnej firmy związanej z przemysłem i medycyną możliwości i drogi rozwoju oraz stworzenie forum wymiany doświadczeń, pozyskania kontaktów oraz poszukiwania funduszy na prowadzenie działań w zakresie innowacji i ich wdrażania.

Patronat Honorowy:
JM Rektor Uniwersytetu Rzeszowskiego – prof. dr hab. Sylwester CZOPEK
JM Rektor Politechniki Rzeszowskiej – prof. dr hab. inż. Piotr KOSZELNIK

Przewodniczący Konferencji i Komitetu Organizacyjnego:
dr inż. Paweł TUREK

Zastępcy Przewodniczącego:
dr inż. Łukasz PRZESZŁOWSKI
dr n. med. Damian FILIP

Konferencja będzie poświęcona edukacji oraz inspiracji studentów, naukowców i kadry akademickiej kierunków medycznych i inżynieryjnych do realizacji interdyscyplinarnych badań naukowych w zakresie innowacyjnych technologii w medycynie, nawiązywanie współpracy pomiędzy przedstawicielami świata nauki i biznesu, stworzenie forum wymiany doświadczeń oraz wskazanie możliwości i kierunków rozwoju.

Tematyka konferencji:
* Systemy szybkiego prototypowania i ich zastosowanie w medycynie
* Medycyna pola walki
* Wirtualna rzeczywistość w aspekcie medycznym
* Ratownictwo medyczne
* Techniki komputerowe w bioinżynierii
* Projektowanie i badania innowacyjności biomateriałów
* Metrologia medyczna
* Nowoczesne metody obrazowania medycznego, hybrydowe techniki obrazowania
* Inżynieria rehabilitacyjna
* Technologie druku 3D/4D w wytwarzaniu implantów i sztucznych narządów
* Materiały dla medycyny
* Technologie mobilne w medycynie

Ważne terminy:
Zgłoszenie udziału w konferencji – **05.09.2023 r.**
Termin załączania abstraktów – **02.10.2023 r.**
Miejsce konferencji: Urban Lab, 3 Maja 13, 35-030 Rzeszów

medycyna40.prz.edu.pl